

Image analysis for Alzheimer’s disease prediction: Embracing pathological hallmarks for model architecture design

Sarah C. Brüningk*, Felix Hensel*, Catherine R. Jutzeler**, Bastian Rieck**

Department of Biosystems Science and Engineering, ETH Zurich and SIB Swiss Institute of Bioinformatics.

*: These authors contributed equally. **: These authors share last authorship.

Abstract

Alzheimer’s disease (AD) is associated with local (e.g. brain tissue atrophy) and global brain changes (loss of cerebral connectivity), which can be detected by high-resolution structural magnetic resonance imaging. Conventionally, these changes and their relation to AD are investigated independently. Here, we introduce a novel, highly-scalable approach that simultaneously captures *local* and *global* changes in the diseased brain. It is based on a neural network architecture that combines patch-based, high-resolution 3D-CNNs with global topological features, evaluating multi-scale brain tissue connectivity. Our local-global approach reached competitive results with an average precision score of 0.95 ± 0.03 for the classification of cognitively normal subjects and AD patients (prevalence $\approx 55\%$).

1. Introduction

Affecting an estimated 35 million people worldwide, Alzheimer’s disease (AD) is the leading cause ($\approx 70\%$) of dementia in elderly people (Winblad et al., 2016). AD is a chronic progressive disease, neuropathologically hallmarked by amyloid plaques, neurofibrillary tangles, glial responses, as well as neuronal and synaptic loss (Scheff et al., 2006; Serrano-Pozo et al., 2011; Suemoto et al., 2017). As the disease progresses, these pathological processes trigger large-scale changes to the brain morphology, including atrophy, loss of cere-

bral connectivity, and volumetric shrinkage of distinct brain areas (e.g. amygdala and hippocampus). Using magnetic resonance imaging (MRI), these morphological changes can be quantified (Rosenbloom and Pfefferbaum, 2008), both locally at high resolution (small scale atrophy) and globally throughout the image (tissue connectivity). Machine learning has frequently been applied for MRI image classification and discovery of early imaging biomarkers of AD. Convolutional Neural Networks (CNNs) are widely used for these tasks (Jo et al., 2019). Owing to the high resolution three dimensional (3D) MRI images, training of deep 3D-CNNs on the full image space is computationally expensive. Alternatively, MRI images have been down-sampled at the cost of lower resolution (Jin et al., 2019; Korolev et al., 2017; Oh et al., 2019) or patch-based CNNs have been applied (Ahmed et al., 2019; Lin et al., 2018; Liu et al., 2018a,b) that are limited in detecting global, whole-image features. We propose to address the trade-off between image resolution and computational cost through topological data analysis (TDA). TDA is a rapidly developing field based on algebraic topology that aims to study the shape of complex data. One of its flagship tools is *persistent homology* (PH). Enjoying stability properties and robustness against noise, PH captures multi-scale information on the connectivity of a data set, such as connected components, cycles, and higher-dimensional voids. In recent years, TDA has been successfully

combined with machine learning methods; e.g. Hofer et al. (2017). The aim of this study is to combine local and global neuroimaging features to capture the full spectrum of AD-induced brain changes with the overarching aim of improving the understanding of this disease and to provide a scalable solution to the challenge of 3D-image analysis. Two approaches, an ensemble of patch-based 3D-CNNs, and a combination of TDA with a single patch 3D-CNN were investigated. A deliberately simple CNN architecture was chosen as baseline in this preliminary study.

2. Methods

Data selection and preprocessing We included structural T1-weighted, MR images (no contrast) from the **Alzheimer’s Disease Neuroimaging Initiative** (ADNI) for AD patients and healthy controls (CN) of matched age groups. Data from all ADNI subcohorts (ADNI1, 2, 3, and GO) were used. For details on the data selection and preprocessing, see Appendix A.1.

Convolutional neural network Preprocessed images were rescaled ($193 \times 229 \times 193$ voxels), cropped ($180 \times 216 \times 180$), and cut into 216 patches of size $30 \times 36 \times 30$ - a trade-off between image detail captured and computational cost. Hyperparameters of a 3D-CNN (see Figure 1, 3DCNN-P) were optimised by random sampling on a patch within the hippocampus, denoted as 3DCNN-P*. Models using these optimal hyperparameters were trained independently on each image patch within 2500 epochs with early stopping based on validation loss using the Adam optimiser with He uniform initialisation. Our method is implemented in Python using Keras/TensorFlow; we plan on making our implementation publicly available.

Topological features For 3D MR images, topological features can occur in dimen-

sions 0 (connected components), 1 (cycles), and 2 (voids). We follow recent work (Rieck et al., 2020), which proposed: 1. calculating persistent homology, and 2. vectorising the resulting descriptors via *persistence images* (Adams et al., 2017, PI), thus simplifying their integration into neural networks; we refer to Edelsbrunner and Harer (2010) for a comprehensive introduction to TDA. Classification based on topological features was performed using a 2D-CNN as outlined in Figure 1. Following hyperparameter optimisation, only 1-dimensional features were used, as they yielded the best performance. We tested several preprocessing steps on the MRI images (Gaussian filtering, down-sampling, filtering out low-persistence features, calculating both sublevel-sets and superlevel-sets) and of these report the best results to date.

Ensemble models Two approaches were considered that combined local and global imaging features through using i) all 216 image patches, or ii) a single image patch with PI representation of the full image. For i), class probabilities for each subject and model were normalised, and centred around a decision boundary of zero and served as input for logistic regression (LR) with grid search optimised hyperparameters. For ii), the preclassification encodings of the individually trained 2D/3D-CNNs (3D-CNN-P* and 2D-CNN-PI) were combined through a single fully connected layer with optimized l1 regularization and sigmoidal activation (see Figure 1).

Performance evaluation We performed 4-fold cross validation (CV) splitting patients into training (80%) and validation (20%) sets, stratified by class labels. All longitudinal images per subject were used for training and a single image, randomly selected from the longitudinal set, was selected for each validation patient. Depending on the split, 851–895/291–298 train and 73–74/73–74 validation images/subjects were used with an aver-

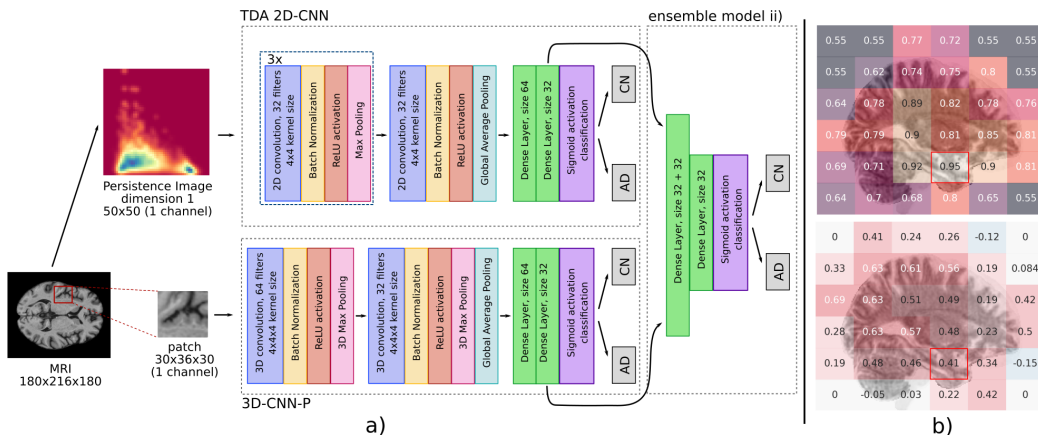


Figure 1: a) TDA 2D- and 3D-CNN architectures with ensemble model ii) using the pre-classification layer encodings in a fully connected layer. b) APS (five run average, top) and normalised, centred class probabilities for one AD patient (single run, bottom) serving as features in ensemble ii) overlaid to a sagittal slice of the MR image. The image patch giving the best classification accuracy is highlighted.

age validation prevalence of AD of $54.6 \pm 0.5\%$. Independent of the model architecture, training was repeated four times (runs) for each CV fold. We averaged all metrics over individual runs, then over folds, reporting mean values with standard deviations. A Wilcoxon signed rank test was performed to evaluate statistical significance.

3. Results

Table 1 gives an overview of the classification performance of the different architectures investigated. The performance of a single patch based 3D-CNN was strongly influenced by the anatomical location of the image patch as shown in Figure 1b). The best-performing model (denoted as 3D-CNN-P*) was obtained for a patch at the base of the brain encompassing parts of the left hippocampus and amygdala, two structures whose changes have previously been reported as potential AD imaging biomarkers (Poulin et al., 2011). Patches containing parts of

other AD associated brain structures, such as the thalamus, caudate, or the ventricles also yielded competitive classification results. Classification performance of any TDA-based model alone was influenced by the model PI preprocessing. So far, the best results in terms of APS were achieved with a superlevel PI input ($APS = 0.79 \pm 0.04$). None of the tested TDA-based approaches was superior to 3D-CNN-P*. Ensemble model i) combining the predictions of all 216 3D-CNN-Ps had an improved classification performance in terms of APS relative to the best single patch model, 3D-CNN-P*, yet differences were not significant ($p > 0.05$). So far, no statistically significant difference between 3D-CNN-P* and the 3D-CNN-P*-TDA ensemble ii) were observed ($p > 0.05$).

4. Discussion and Conclusions

The macroscopic and microscopic brain changes related to AD provide a strong incentive for the combination of local and global

Local	3D-P*			3D-P*	3D-P*	3D-P
Global		2D-PI-sup	2D-PI-rs2	2D-PI-sup	2D-PI-rs2	LR
ACC	0.85 ± 0.06	0.76 ± 0.02	0.75 ± 0.01	0.86 ± 0.06	0.86 ± 0.05	0.88 ± 0.04
AUC	0.89 ± 0.05	0.78 ± 0.02	0.78 ± 0.02	0.89 ± 0.04	0.89 ± 0.04	0.93 ± 0.05
APS	0.92 ± 0.03	0.78 ± 0.03	0.79 ± 0.04	0.91 ± 0.03	0.91 ± 0.04	0.95 ± 0.03
Recall	0.87 ± 0.08	0.88 ± 0.08	0.86 ± 0.1	0.89 ± 0.06	0.88 ± 0.08	0.89 ± 0.07
Precision	0.87 ± 0.04	0.74 ± 0.02	0.74 ± 0.03	0.86 ± 0.05	0.87 ± 0.03	0.90 ± 0.02

Table 1: Classification performance using local (patches) and/or global (full image) data. Abbreviations: 2D/3D: 2/3D-CNN, P: All patches, P*: Best single patch, PI-sup: Superlevel PI, PI-rs2: factor two resampled PI.

imaging features for AD detection. Here, we realised this through the combination of a 3D-CNN on a single, high-resolution image patch, in combination with either TDA or a LR ensemble model. We applied state-of-the-art pipelines for image preprocessing, topological descriptor generation, and investigated a number of preprocessing steps for the TDA part of the study. Yet, TDA did not improve classification performance in this preliminary analysis, despite encouraging results from ensemble model ii) which was competitive to previous approaches (Jo et al., 2019; Oh et al., 2019; Pan et al., 2020), motivating the merit of combining features from multiple brain locations. Our topological feature generation, despite the use of standard pipelines, may benefit from further refinements to capture more representative global connectivity features. We plan on investigating methods of filtering out topological noise, e.g. through image smoothing, or the use of different data descriptors. Independent of the ensemble mode used, our approach is highly parallelizable, fast (1 s/0.1 s per epoch for 3D/2D-CNN training), and based on a simple architecture that permits interpretability analysis to elucidate the underlying biological hallmarks driving classification—a task we want to pursue in the future. AD-CN classification may be considered a simple task with limited clinical application given reliable other means of classification such as neuropsychological eval-

uation. However, we deliberately chose this imaging-based classification task to serve as a starting point for future evaluations as it is not prone to label uncertainties and can serve as input for transfer learning to classify mildly cognitively impaired patients vs AD. Finally, an important comparison will be that with a 3D-CNN trained on the full, high-resolution MRI image. Insufficient GPU memory currently limits this baseline comparison for us, which stresses the importance of providing *scalable* solutions for high-resolution 3D data analysis using CNNs. We attempted training a 3D-CNN on a down-sampled (97×115×97) image, but were restricted to a small (< 5) batch size and slow training (60 s per epoch) on the same hardware, preventing proper hyperparameter selection. Due to the large image volume, identification of localized disease markers may also require a larger ratio of training examples to model parameters than available in this study. A clear advantage of the presented patch-based implementation is its scalability, permitting parallelized training on different image patches that is easily conductable using state-of-the-art GPU servers with standard GPU memory. We suggest that the presented architecture may easily translate to other clinical indications employing image-based classification and, following further optimization, could help to tackle the trade-off between computational cost and imaging details retained for classification.

Acknowledgements

This work was partially funded and supported by the National Institutes of Health (S.C.B., C.R.J); Ambizione Grant #PZ00P3186101, C.R.J). The content provided here is solely the responsibility of the authors and does not necessarily represent the official views of the funding agencies. The funders had no role in study design, data collection & analysis, decision to publish, or preparation of the manuscript. Data collection and sharing for this project was funded by the Alzheimer's Disease Neuroimaging Initiative (ADNI) (National Institutes of Health Grant U01 AG024904) and DOD ADNI (Department of Defense award number W81XWH-12-2-0012). ADNI is funded by the National Institute on Aging, the National Institute of Biomedical Imaging and Bioengineering, and through generous contributions from the following: AbbVie, Alzheimer's Association; Alzheimer's Drug Discovery Foundation; Araclon Biotech; BioClinica, Inc.; Biogen; Bristol-Myers Squibb Company; CereSpir, Inc.; Cogstate; Eisai Inc.; Elan Pharmaceuticals, Inc.; Eli Lilly and Company; EuroImmun; F. Hoffmann-La Roche Ltd and its affiliated company Genentech, Inc.; Fujirebio; GE Healthcare; IXICO Ltd.; Janssen Alzheimer Immunotherapy Research & Development, LLC.; Johnson & Johnson Pharmaceutical Research & Development LLC.; Lumosity; Lundbeck; Merck & Co., Inc.; Meso Scale Diagnostics, LLC.; NeuroRx Research; Neurotrack Technologies; Novartis Pharmaceuticals Corporation; Pfizer Inc.; Piramal Imaging; Servier; Takeda Pharmaceutical Company; and Transition Therapeutics. The Canadian Institutes of Health Research is providing funds to support ADNI clinical sites in Canada. Private sector contributions are facilitated by the Foundation for the National Institutes of Health (www.fnih.org). The grantee organization is the Northern California Institute for Research and Education, and

the study is coordinated by the Alzheimer's Therapeutic Research Institute at the University of Southern California. ADNI data are disseminated by the Laboratory for Neuro Imaging at the University of Southern California.

References

- Henry Adams, Tegan Emerson, Michael Kirby, Rachel Neville, Chris Peterson, Patrick Shipman, Sofya Chepushtanova, Eric Hanson, Francis Motta, and Lori Ziegelmeier. Persistence images: a stable vector representation of persistent homology. *J. Mach. Learn. Res.*, 18:Paper No. 8, 35, 2017. ISSN 1532-4435.
- Samsuddin Ahmed, Kyu Yeong Choi, Jang Jae Lee, Byeong C. Kim, Goo Rak Kwon, Kun Ho Lee, and Ho Yub Jung. Ensembles of Patch-Based Classifiers for Diagnosis of Alzheimer Diseases. *IEEE Access*, 7:73373–73383, 2019. ISSN 21693536. doi: 10.1109/ACCESS.2019.2920011.
- Herbert Edelsbrunner and John L. Harer. *Computational topology*. American Mathematical Society, Providence, RI, 2010. ISBN 978-0-8218-4925-5. doi: 10.1090/mbk/069. An introduction.
- Christoph Hofer, Roland Kwitt, Marc Niethammer, and Andreas Uhl. Deep learning with topological signatures. In I. Guyon, U. V. Luxburg, S. Bengio, H. Wallach, R. Fergus, S. Vishwanathan, and R. Garnett, editors, *Advances in Neural Information Processing Systems 30*, pages 1634–1644. Curran Associates, Inc., 2017.
- Dan Jin, Jian Xu, Kun Zhao, Fangzhou Hu, Zhengyi Yang, Bing Liu, Tianzi Jiang, and Yong Liu. Attention-based 3D Convolutional Network for Alzheimer's Disease Diagnosis and Biomarkers Exploration. In *2019 IEEE 16th International Symposium*

- on *Biomedical Imaging (ISBI 2019)*, pages 1047–1051. IEEE, 2019. ISBN 978-1-5386-3641-1. doi: 10.1109/ISBI.2019.8759455.
- Taeho Jo, Kwangsik Nho, and Andrew J. Saykin. Deep learning in alzheimer's disease: Diagnostic classification and prognostic prediction using neuroimaging data. *Frontiers in Aging Neuroscience*, 11:220, 2019. ISSN 1663-4365. doi: 10.3389/fnagi.2019.00220.
- Sergey Korolev, Amir Safiullin, Mikhail Belyaev, and Yulia Dodonova. Residual and plain convolutional neural networks for 3D brain MRI classification. *Proceedings - International Symposium on Biomedical Imaging*, pages 835–838, 2017. ISSN 19458452. doi: 10.1109/ISBI.2017.7950647.
- Weiming Lin, Tong Tong, Qinquan Gao, Di Guo, Xiaofeng Du, Yonggui Yang, Gang Guo, Min Xiao, Min Du, and Xiaobo Qu. Convolutional Neural Networks-Based MRI Image Analysis for the Alzheimer's Disease Prediction From Mild Cognitive Impairment. *Frontiers in Neuroscience*, 12 (NOV):1–13, 2018. ISSN 1662-453X. doi: 10.3389/fnins.2018.00777.
- Mingxia Liu, Jun Zhang, Ehsan Adeli, and Dinggang Shen. Landmark-based deep multi-instance learning for brain disease diagnosis. *Medical Image Analysis*, 43: 157–168, 2018a. ISSN 13618423. doi: 10.1016/j.media.2017.10.005.
- Mingxia Liu, Jun Zhang, Dong Nie, Pewthian Yap, and Dinggang Shen. Anatomical Landmark Based Deep Feature Representation for MR Images in Brain Disease Diagnosis. *IEEE Journal of Biomedical and Health Informatics*, 22(5):1476–1485, 2018b. ISSN 2168-2194. doi: 10.1109/JBHI.2018.2791863.
- Kanghan Oh, Young Chul Chung, Ko Woon Kim, Woo Sung Kim, and Il Seok Oh. Classification and Visualization of Alzheimer's Disease using Volumetric Convolutional Neural Network and Transfer Learning. *Scientific Reports*, 9(1):1–16, 2019. ISSN 20452322. doi: 10.1038/s41598-019-54548-6.
- Dan Pan, An Zeng, Longfei Jia, Yin Huang, Tory Frizzell, and Xiaowei Song. Early Detection of Alzheimer's Disease Using Magnetic Resonance Imaging: A Novel Approach Combining Convolutional Neural Networks and Ensemble Learning. *Frontiers in Neuroscience*, 14:259, 2020. ISSN 1662-453X. doi: 10.3389/fnins.2020.00259.
- Stéphane P. Poulin, Rebecca Dautoff, John C. Morris, Lisa Feldman Barrett, and Bradford C. Dickerson. Amygdala atrophy is prominent in early Alzheimer's disease and relates to symptom severity. *Psychiatry Research - Neuroimaging*, 194(1):7–13, 2011. ISSN 09254927. doi: 10.1016/j.psychres.2011.06.014.
- Bastian Rieck, Tristan Yates, Christian Bock, Karsten Borgwardt, Guy Wolf, Nicholas Turk-Browne, and Smita Krishnaswamy. Uncovering the topology of time-varying fMRI data using cubical persistence. *arXiv pre-print arXiv:2006.07882*, 2020.
- Margaret J Rosenbloom and Adolf Pfefferbaum. Magnetic resonance imaging of the living brain: evidence for brain degeneration among alcoholics and recovery with abstinence. *Alcohol Research & Health*, 2008.
- Stephen W Scheff, Douglas A Price, Frederick A Schmitt, and Elliott J Mufson. Hippocampal synaptic loss in early alzheimer's disease and mild cognitive impairment. *Neurobiology of aging*, 27(10):1372–1384, 2006. doi: 10.1016/j.neurobiolaging.2005.09.012.
- Alberto Serrano-Pozo, Matthew P Frosch, Eliezer Masliah, and Bradley T Hyman.

Neuropathological alterations in alzheimer disease. *Cold Spring Harbor perspectives in medicine*, 1(1):a006189, 2011. doi: 10.1101/cshperspect.a006189.

Claudia K Suemoto, Renata EL Ferretti-Rebustini, Roberta D Rodriguez, Renata EP Leite, Luciana Soterio, Sonia MD Brucki, Raphael R Spera, Tarcila M Cipiciani, Jose M Farfel, Alexandre Chiavegatto Filho, et al. Neuropathological diagnoses and clinical correlates in older adults in brazil: A cross-sectional study. *PLoS medicine*, 14(3):e1002267, 2017. doi: 10.1371/journal.pmed.1002267.

Bengt Winblad, Philippe Amouyel, Sandrine Andrieu, Clive Ballard, Carol Brayne, Henry Brodaty, Angel Cedazo-Minguez, Bruno Dubois, David Edvardsson, Howard Feldman, et al. Defeating alzheimer's disease and other dementias: a priority for european science and society. *The Lancet Neurology*, 15(5):455–532, 2016. doi: 10.1016/S1474-4422(16)00062-4.

Appendix A. Supplements

A.1. Preprocessing of MRI data

We included all T1-weighted MRI images from ADNI1, 2, 3, and GO, which were captured and preprocessed by ADNI. Results included in our work come from pre-processing performed using `fMRIPrep` 20.1.1, a `Nipype` 1.5.0 based tool. All MRIs were corrected for intensity non-uniformity (INU) with `N4BiasFieldCorrection`, distributed with ANTs 2.2.0, and used as T1w-reference throughout the workflow. The T1w-reference was then skull-stripped with a `Nipype` implementation of the `antsBrainExtraction.sh` workflow (from ANTs), using `OASIS30ANTs` as a target template. Volume-based spatial normalisation to a standard coordinate space (`MNI152NLin2009cAsym`) was performed through nonlinear registration with `antsRegistration`, using brain-extracted versions of both T1w reference and the T1w template. We selected the template ‘ICMB 152 Nonlinear Asymmetrical Template Version 2009c’ for spatial normalisation.

Many internal operations of `fMRIPrep` use the `Nilearn` library, version 0.6.2, mostly within the functional processing workflow. For more details of the pipeline, please refer to [the official documentation of fMRIPrep](#). Preprocessing was finalised by intensity normalisation of the extracted and MNI space registered brain images.